JLAB-THY-15-xxxx

Constraints on large-x parton distributions from new weak boson production and deep-inelastic scattering data

(Dated: September 14, 2015)

Abstract

We present a new set of leading twist parton distribution functions (PDFs), which take advantage of developments in the theoretical treatment of nuclear corrections as well as new data. The analysis includes for the first time data on the free neutron structure function from the BONuS experiment at Jefferson Lab, and new charged lepton and W-boson asymmetry data from Fermilab, which significantly reduce the uncertainty on the d/u ratio at large values of x.

I. INTRODUCTION

[XXX to edit]

... general intro ...

... what is new since CJ12 ...

• more complete/consistent/systematic treatment of nuclear corrections esp. nucleon off-shell corrections

• impact of new W-boson asymmetry data on d/u ratio

• inclusion of JLab (BONuS) data

• analysis of $\bar{d} - \bar{u}$ at large x ... choose either $\bar{d}/\bar{u} \to 1$ or 0 as $x \to 1$ ...

• S-ACOT scheme for heavy quarks

• LO fit

• α_s treatment

... In Sec. II we ...

II. THEORETICAL FOUNDATIONS

In this section we present the theoretical framework that is used for the CJ15 analysis.

A. PDF parametrizations [XXX to edit]

• For the parametrization of the PDFs at the input scale Q_0^2, a common form has been adopted for all parton species f,

$$xf(x, Q_0^2) = a_0 x^{a_1} (1-x)^{a_2} (1 + a_3 \sqrt{x} + a_4 x). \tag{1}$$

This form applies to the valence distributions $xq_v \equiv x(q - \bar{q})$, for $q = u$ and d, the isoscalar and isovector sea quark distributions $x(\bar{u} + \bar{d})$ and $x(\bar{d} - \bar{u})$, and the gluon distribution xg. However, to allow for a more flexible parametrization of the valence d_v PDF in the large-x region, we add in a small admixture of the u_v PDF,

$$d_v \to a_0^{d_v} \left(\frac{d_v}{a_0^{d_v}} + b\, x^c u_v \right), \tag{2}$$

with b and c as two additional parameters. The result of this modification is that $d_v/u_v \to a_0^{d_v}\, b$ as $x \to 1$, provided $a_2^{d_v} > a_2^{u_v}$, which is usually the case. A finite, nonzero value of this

ratio is indeed expected in several nonperturbative models of hadron structure [6–8]. It is also required from a purely practical point of view, as it avoids potentially large biases on the d-quark PDF central value [14], as well as on its PDF error estimate, as we discuss in detail in Sec. IV. The a_0 parameters for the u_v and d_v distributions are fixed by the appropriate valence quark number sum rules, while a_0^g is fixed by the momentum sum rule.

- For the input scale Q_0 we choose the charm quark scale, $Q_0 = m_c$.
- New parametrization for $\bar{d} - \bar{u}$ ... avoids negative PDFs? ...

In our analysis we parametrize the $\bar{d}/\bar{u}$ ratio as

$$\frac{\bar{d}}{\bar{u}} \;=\; a_0 x^{a_1}(1-x)^{a_2} + 1 + x^{a_3}(1-x)^{a_4}, \tag{3}$$

which ensures that in the limit $x \to 1$ one has $\bar{d}/\bar{u} \to 1$. The existing data are not able to reliably determine the large-x behavior of the ratio, so as an alternative we also perform fits using $\bar{d}/\bar{u} = a_0 x^{a_1}(1-x)^{a_2} + (1 + x^{a_3})(1-x)^{a_4}$, which vanishes in the $x \to 1$ limit. The $\bar{d}/\bar{u} \to 1$ limit is what would be expected from perturbative QCD, while the $\bar{d}/\bar{u} \to 0$ limit may arise if the trend in $x \gtrsim 0.3$ points from the E866 experiment [29] were to continue to larger x.

...[ARE PARAMETERS IN TABLE I FOR $\bar{d}/\bar{u}$ OR $\bar{d} - \bar{u}$???]...

- The strange quark distribution is not well constrained by existing data ...[SOME DISCUSSION OF ISSUES]... For the strange quark PDF, we follow our previous analyses [14, 15] by assuming flavor independence of the shape of the sea quark PDFs, and consequently take a fixed ratio

$$\kappa \;=\; \frac{s + \bar{s}}{\bar{u} + \bar{d}}, \tag{4}$$

with the further assumption that $\bar{s} = s$. In this study we take $\kappa = 0.4$.

B. Heavy quarks [JFO?? to edit]

- Implementation of S-ACOT scheme.
- In our analysis we take the masses of the charm and bottom quarks to be $m_c = 1.3$ GeV and $m_b = 4.5$ GeV, respectively.
- The 4-flavor value of the QCD cutoff scale used in this analysis is $\Lambda^{(4)}_{\rm QCD} = 226.8$ MeV.

C. $1/Q^2$ corrections [XXX to edit]

• For target mass corrections, use of OPE (G-P); ... comparisons with EFP, series expansion; ... in practice doesn't matter!(?)

• ... give formula for TMC in F_2 ???

• For other subleading $1/Q^2$ corrections, such as higher twist and other residual power corrections ...

$$F_2(x,Q^2) = F_2^{(\mathrm{LT+TMC})}(x,Q^2)\left(1+\frac{C_{\mathrm{HT}}(x)}{Q^2}\right), \tag{5}$$

where $F_2^{(\mathrm{LT+TMC})}$ denotes the leading twist structure function including TMCs. For simplicity we generically refer to the fitted $1/Q^2$ term as a "higher twist" correction, and parametrize the higher twist coefficient function by

$$C_{\mathrm{HT}}(x) = h_0 x^{h_1}(1+h_2 x), \tag{6}$$

assuming it to be isospin independent (see, however, Refs. [62–65]).

D. Nuclear corrections

As in the previous CJ PDF analyses [11, 14, 15], the use of deuterium DIS and Drell-Yan data necessitates taking into account the differences between PDFs in the deuteron and those in the free proton and neutron. The CJ15 analysis follows a similar approach, with several improvements over the earlier implementations, as we discuss in the following. While the earlier analyses applied nuclear corrections only to deep-inelastic deuteron structure functions, here we formulate the corrections at the parton level and generalize the treatment to any process involving quark, antiquark or gluon PDFs in the deuteron.

Generally, the nuclear corrections in high energy reactions account for Fermi motion, binding and nucleon off-shell effects, which are implemented in the form of convolutions using nuclear smearing functions. These become increasingly important at intermediate and large values of x, and will be the focus of our attention in this section. In addition, rescattering effects mediated by Pomeron and pion exchange mechanisms give rise to shadowing at small values of x ($x \lesssim 0.1$) [1, 2] and a small amount of antishadowing at $x \sim 0.1$ [1, 3]. In

practice, however, the shadowing and antishadowing corrections are very small, and have negligible effect on the phenomenology in our analysis.

1. *Nuclear smearing*

From the standard nuclear impulse approximation for the scattering of a projectile (lepton or hadron) from a deuteron d, the momentum distribution of a parton inside the deuteron is given by a convolution of the corresponding PDF in the bound nucleon and a light-cone momentum distribution $f_{N/d}$ of nucleons in the deuteron (or "smearing function"). Taking for illustration the PDF for a quark of flavor q (the generalization to antiquarks and gluons is straightforward), its momentum distribution function in the deuteron can be computed as [66, 67]

$$q^d(x,Q^2) \;=\; \int \frac{dz}{z} dp^2 \, f_{N/d}(z,p^2)\, \widetilde{q}^N(x/z,p^2,Q^2), \tag{7}$$

where $z = (M_d/M)(p\cdot q/p_d\cdot q)$ is the nucleon momentum fraction in the deuteron, with p and p_d the four-momenta of the nucleon and deuteron, respectively, and M_d is the deuteron mass. The nucleon virtuality p^2 defines the degree to which the bound nucleon is off its mass shell, $p^2 \neq M^2$, and the function $\widetilde{q}^N$ represents the quark PDF in the off-shell nucleon. For the isoscalar deuteron, a sum over the nucleons $N = p, n$ is implied.

While the off-shell nucleon PDF $\widetilde{q}^N$ is not by itself an observable, its dependence on the virtuality p^2 can be studied within a given theoretical framework. Since the bound state effects in the deuteron are the smallest of all the atomic nuclei, one may expand the off-shell nucleon distribution to lowest order about its on-shell limit [67, 68],

$$\widetilde{q}^N(x,p^2,Q^2) \;=\; q^N(x,Q^2)\left(1 + \frac{p^2-M^2}{M^2}\delta f^N(x,Q^2)\right), \tag{8}$$

where the coefficient of the off-shell term is given by

$$\delta f^N(x,Q^2) \;=\; \left.\frac{\partial \ln \widetilde{q}^N(x,p^2,Q^2)}{\partial \ln p^2}\right|_{p^2=M^2}. \tag{9}$$

The on-shell term in Eq. (8) leads to the standard on-shell convolution representation for the nuclear PDF, while the off-shell term can be evaluated as an additive correction. Defining the total quark PDF in the deuteron as the sum of the on-shell and off-shell contributions,

$q^d = q^{d\,(\rm on)} + q^{d\,(\rm off)}$, the two components can be written as

$$q^{d\,(\rm on)}(x,Q^2) \;=\; \int \frac{dz}{z} f^{(\rm on)}(z)\, q^N(x/z,Q^2), \tag{10a}$$

$$q^{d\,(\rm off)}(x,Q^2) \;=\; \int \frac{dz}{z} f^{(\rm off)}(z)\, \delta f^N(x/z,Q^2)\, q^N(x/z,Q^2). \tag{10b}$$

The on-shell and off-shell smearing functions $f^{(\rm on)}$ and $f^{(\rm off)}$ are taken to be the same for the proton and neutron (isospin symmetry breaking effects are not expected to be significant) and are given by [71]

$$f^{(\rm on)}(z) \;=\; \int dp^2\, f_{N/d}(z,p^2), \tag{11a}$$

$$f^{(\rm off)}(z) \;=\; \int dp^2\, \frac{p^2-M^2}{M^2}\, f_{N/d}(z,p^2). \tag{11b}$$

A systematic method for computing the smearing functions is within the weak binding approximation (WBA), in terms of the deuteron wave function [69, 70]. For large $Q^2 \to \infty$ the on-shell smearing function $f^{(\rm on)}$ has a simple probabilistic interpretation in terms of the light-cone momentum fraction $z \to 1 + (\varepsilon + \gamma\, p_z)/M)$ of the deuteron carried by the struck nucleon, where $\varepsilon = p_0 - M$ is the separation energy. At finite Q^2, however, the smearing functions depends also on the parameter $\gamma^2 = 1 + 4x^2M^2/Q^2$, which characterizes the deviation from the Bjorken limit.

For the deuteron wave functions we consider several modern potentials based on high-precision fits to nucleon–nucleon scattering data. The models differ primarily in their treatment of the short range NN interaction, while the long range part of the wave functions is constrained by the chiral symmetry of QCD and parametrized through one-pion exchange. Specifically, the nonrelativistic AV18 [72] and CD-Bonn [73] NN potential models (which fit around 3,000 data points in terms of ≈ 40 parameters), and the more recent relativistic WJC-1 and WJC-2 [74] potentials (which describe almost 4,000 data points in terms 27 and 15 parameters, respectively), provide wave functions with a representative spread of behaviors in the low and high momentum regions. Of these, the CD-Bonn wave function has the softest momentum distribution, while the WJC-1 wave function has the hardest, with the others lying between the two. The differences in the strength of the high-momentum tails of the wave functions are reflected in differences between the behaviors of the nuclear corrections at large values of x. Note that the effects of the nuclear smearing corrections are not suppressed at large Q^2, and must be considered at all scales wherever data at $x \gtrsim 0.3$ are used [11–13].

2. *Nucleon off-shell corrections*

While the effects of the nuclear smearing are relatively well understood, at least in the sense that they can be directly related to the properties of the deuteron wave function, the nucleon off-shell correction in Eqs. (8) and (9) is much more uncertain and model dependent. In the literature a number of model studies have been performed to estimate the modification of PDFs in bound nucleons relative to the free nucleon PDFs [66–69, 75–79], some of which have been motivated by the original observation of the nuclear EMC effect.

Some early studies of off-shell corrections to PDFs were based on spectator quark models [66–69, 76], in which the scattering takes place from a quark that is accompanied by a "diquark" system (proton with a quark removed) that is spectator to the deep-inelastic collision. The scattering amplitude was represented through a quark spectral function characterized by an ultraviolet momentum cutoff scale Λ and an invariant mass of the spectator system, both of which were fixed by comparing with the on-shell structure function data.

The effects of nucleon off-shell corrections on global PDF analysis were first explored in Ref. [11] using a simple analytic parametrization of the corrections computed in the relativistic quark spectator model of Ref. [76]. In the subsequent CJ11 analysis [14] a more elaborate off-shell model was considered [69], in which the corrections were related to the change in the nucleon's confinement radius in the nuclear medium, as well as the average virtuality of the bound nucleons. The change in the confinement radius (or nucleon "swelling") was varied between 1.5% and 1.8%, and the virtuality of the bound nucleons $\langle p^2 - M^2\rangle/M^2 \equiv \int dz\, f^{(\rm off)}(z)$ ranged from -3.6% to -6.5% for the four deuteron wave functions discussed above.

Most recently, the CJ12 PDF analysis [15] further took into account the correlations between the nucleon swelling and the deuteron wave function, defining a set of nuclear corrections that ranged from mild (for the hardest, WJC-1 wave function [74] coupled to a small, 0.3% nucleon swelling) to strong (for the softest, CD-Bonn wave function [73] with a large, 2.1% swelling parameter). The entire range of nuclear corrections was consistent with the existing experimental data, with each set giving essentially the same χ^2 values for the global fit, $\chi^2/{\rm dof} \approx 1.03$.

As noted, in all the previous studies the off-shell corrections were implemented only for the deuteron F_2^d structure function and in the valence quark approximation. To apply the

model to observables that are sensitive to both the valence and sea sectors, Ehlers *et al.* [71] generalized the single-pole approximation to the spectral function to allow different off-shell behaviors of the valence quark, sea quark and gluon distributions. The three corresponding spectator state masses ("qq" for valence quarks, "$qq\bar{q}q$" for sea quarks, and "qqq" for gluons) were then fitted to the isoscalar valence, sea quark and gluon PDFs in the free nucleon. This allowed nucleon off-shell corrections to be applied to other observables, such as the deuteron F_L^d structure function or proton–deuteron Drell-Yan cross sections. The only free parameter in this model, which we refer to as the "off-shell covariant spectator" (OCS) model, is the rescaling parameter $\lambda = \partial \log \Lambda^2 / \partial \log p^2$, evaluated at $p^2 = M^2$. The parameter λ can then be included as a parameter in the fit, with errors propagated along with those of the other leading twist parameters in the fit.

As an alternative to modeling the off-shell correction through quark-level amplitudes and parameters, Kulagin and Petti [69] proposed a purely phenomenological parametrization for the off-shell function δf^N of the form

$$\delta f^N \;=\; C(x - x_0)(x - x_1)(1 + x_0 - x). \tag{12}$$

From the constraint that the off-shell correction does not modify the number of valence quarks in the nucleon,

$$\int_0^1 dx\, \delta f^N(x)\, (q(x) - \bar{q}(x)) \;=\; 0, \tag{13}$$

one can infer that the function δf^N must have one or more zeros in the physical range between $x = 0$ and 1. In practice we fit the zero crossing parameter x_0 and the normalization C, which then allows the second zero crossing x_1 to be determined from Eq. (13) analytically. In Ref. [69] these parameters were constrained by fitting to ratios of nuclear to deuteron structure function data, for a range of nuclei up to ^{207}Pb. This resulted in a combined nuclear correction that produced a typical EMC ratio shape, including an $\approx 1\%$ antishadowing enhancement of the F_2^d/F_2^N ratio at $x \approx 0.1 - 0.2$. In contrast, in the present analysis we fit the off-shell parameters by considering only deuterium cross section data.

E. PDF Errors [AA/JFO?? to edit]

... as for CJ12 ... Hessian ... tolerance ...

III. DATA

[XXX to edit]

The CJ15 PDFs are obtained by fitting to a global database of 4035 data points from a variety of high energy scattering processes, listed in Table I. These include deep-inelastic scattering data from BCDMS, NMC, SLAC, HERA and Jefferson Lab (JLab); Drell-Yan p and d cross sections from fixed target experiments at Fermilab; W and Z asymmetries, as well as jet and γ+jet cross sections from the CDF and DØ collaborations at the Tevatron. The table also lists the corresponding χ^2 values for each data set. The overall χ^2/dof is 0.979. The fit is slightly better than in our previous CJ12 analysis [15], partly because of the greater flexibility which we have allowed in the current fit for the nucleon off-shell correction.

... do not include HERMES F_2^p data ... because ...

...[FURTHER DESCRIPTIONS OF DATA]...

...[JUSTIFICATION FOR INCLUDING AND OMITTING SPECIFIC DATA SETS]...

IV. RESULTS

In this section we present the results of our global QCD analysis. The quality of the fit to data is illustrated in Figs. 1 and 2, where the inclusive F_2 structure functions of the proton and deuteron are compared with the CJ15 calculations over several decades of Q^2 and x. For the proton F_2^p structure function in Fig. 1, data from BCDMS [23], NMC [24], SLAC [26] and JLab [27] experiments are shown at approximately constant values of x, while for the JLab data (see inset in Fig. 1) the structure functions are presented at fixed scattering angles, with x increasing with Q^2. The agreement for all the sets is excellent ...[???]..., with the exception of ...[???]...

Similar agreement is seen for the deuteron F_2^d structure function in Fig. 2, where measurements from BCDMS [23], SLAC [26] and JLab [27] are compared with the CJ15 results (data from NMC are presented as a ratio to the proton structure function, F_2^d/F_2^p).

...[SHOW OTHER, e.g. HERA, DATA SEPARATELY??]...

A. CJ15 PDFs

The CJ15 PDFs themselves are displayed in Fig. 3 at a scale of $Q^2 = 10$ GeV^2 for the u, d, $\bar{d}+\bar{u}$ and $\bar{d}-\bar{u}$ distributions, and the gluon distribution scaled by a factor 1/10. The central CJ15 PDFs are determined using the AV18 deuteron wave function and the nucleon off-shell parametrization in Eq. (12), with the parameter values and their errors for the leading twist distributions given in Table II. at the input scale Q_0^2. The uncertainty bands on the PDFs correspond to $\Delta\chi^2 = 1$. The parameters without errors have been fixed by sum rules or other constraints. (To avoid rounding errors when using these values in numerical calculations, we give the parameter values to 5 significant figures.) PDFs for other flavors, such as strange and charm, are not shown in Fig. 3. The strange quark PDF is assumed to be proportional to the light antiquark sea in the ratio $\kappa = 0.4$ [see Eq. (4)], while the charm quark distribution is generated perturbatively through Q^2 evolution. While there has been speculation about nonperturbative or intrinsic contributions to PDFs of heavy flavors, there is currently no evidence from global analysis of high energy scattering data to suggest that these are large [93]. Until more conclusive evidence becomes available, in this analysis we follow the conventional approach in setting these to zero. This is in contrast with the light quark sea, for which a nonperturbative component at the input scale is essential to account for the nonzero flavor asymmetry $\bar{d}-\bar{u}$.

...[NOTE VERY ASYMMETRIC ERRORS AT SMALL x]...

The CJ15 PDFs are compared with PDFs from several recent representative NLO global parametrizations in Fig. 4, in the form of ratios to the central CJ15 distributions. Since different PDF analyses typically utilize different criteria for estimating PDF errors, we display the CJ15 errors for the standard $\Delta\chi^2 = 1$ (or tolerance $T = 1$), as well as with errors inflated by a tolerance of $T = 10$ [15]. Generally the MMHT14 [17] and NNPDF3.0 [20] PDF sets have uncertainties that are comparable to the CJ15 PDF errors with $T = 10$, while those for the HERAPDF15 [22] distributions are closer to the CJ15 $T = 1$ errors. This may be expected given that the HERAPDF15 analysis only fits HERA data, and therefore uses the $\Delta\chi^2 = 1$ criterion for generating errors.

As known from most previous analyses, the relative uncertainties on the d-quark PDFs are significantly larger than those on the u-quark PDF, especially at large x. For the $\bar{u}$ and $\bar{d}$ distributions the results from the CJ15 fit are similar to those from the MMHT14 and

NNPDF3.0 analyses, while the HERAPDF15 fit gives significantly different results beyond $x \approx 0.1 - 0.2$. Note that the $\bar{d}/\bar{u}$ ratio is most strongly constrained by the E866 Drell-Yan pp and pd scattering data. For the strange quark PDF, the uncertainties in CJ15 are somewhat smaller than in MMHT14 and NNPDF3.0. This is mostly due to the fact that the CJ15 s-quark PDF is assumed to scale with the light antiquark sea in the ratio $\kappa = 0.4$, while other analyses attempt to constrain s-quark PDF from neutrino data, which typically have much larger uncertainties. The errors on the gluon distribution in the MMHT14 and NNPDF3.0 fits lie somewhere between the $T = 1$ and $T = 10$ CJ15 errors, while the HERAPDF15 uncertainties are comparable to the $T = 1$ CJ15 results, as was the case for the various quark distributions. Uncertainties in other modern PDF analyses, such as CT14 [18], JR14 [49] or ABM11 [47] are generally between the representative sets illustrated in Fig. 4.

...[ANY OTHER COMMENTS ABOUT THE GENERAL FEATURES/ERRORS?]...

B. Nuclear corrections at large x

As observed in Fig. 4, the uncertainty on the d-quark distribution at large x values ($x \gtrsim 0.3$) is generally much larger compared with that on the u-quark PDF. This reflects the considerable greater quantity of high precision proton F_2^p structure function data, which, because of the larger charge on the u quark, is at least an order of magnitude more sensitive to the u-quark PDF than to the d. Traditionally, stronger constraints on the d-quark PDF have been sought from inclusive DIS from the neutron, in which the roles of the u and d quark are reversed relative to the proton. However, the absence of free neutron targets has meant that neutron structure information has had to be extracted from measurements on deuterium nuclei. Unfortunately, at high values of x ($x \gtrsim 0.5$) bound state effects in the deuteron become important, and uncertainties in their computation become increasing large with increasing x.

The effects of nuclear corrections on the PDFs are illustrated in Fig. 5, where fits using several different deuteron wave function models are compared. The distributions are displayed relative to the central CJ15 PDFs which use the AV18 deuteron wave function. All fits employ the phenomenological nucleon off-shell parametrization in Eq. (12), with the parameters given in Table III for the AV18 deuteron wave function. The results using the CD-Bonn or WJC-2 wave function are very similar to those for the AV18 wave function,

while using the WJC-1 model leads to larger differences. In fact, the AV18 and CD-Bonn models give almost identical total χ^2/dof of 0.979, while the WJC-2 model gives 0.980, making these three fits essentially indistinguishable. This suggests that, for the most part, the nucleon off-shell parametrization in Eq. (12) is sufficiently flexible to compensate for changes induced by these wave functions. For the WJC-1 model, which has the hardest momentum distribution, it is more difficult for the off-shell correction to compensate within the constraints of Eq. (12), and this leads to a slightly worse overall fit, with a χ^2/dof value of 0.983.

As expected, the variations due to the nuclear models have the largest effects in the d-quark distribution, which is less constrained by proton data and hence more sensitive to uncertainties in the extracted neutron structure function. The spread in the d PDF at $x = 0.8$ is $\approx 20\%$ for all four wave functions. The variations for the AV18, CD-Bonn and WJC-2 wave functions are generally within the $\Delta\chi^2 = 1$ confidence limit, while the WJC-1 results lie outside the band for the u and d PDFs. In particular, the d-quark PDF for the WJC-1 deuteron model is suppressed at high x relative to that in the other models, which correlates with the harder smearing function $f_{N/d}$ at large values of the nucleon light-cone momentum y and hence a larger F_2^d/F_2^N ratio at high x. Interestingly, one also observes an anti-correlation between the behavior of the d-quark distribution at large x and the gluon distribution. In fact, using the WJC-1 wave functions leads to slight decreases in all the quark PDFs at high x, while the gluon PDF has the opposite trend. The spread in the gluon PDF is $\lesssim 10\%$ for $x < 0.8$, although beyond $x \approx 0.3$ the gluon distribution has a very large uncertainty.

Note that while in Fig. 5 the same functional form from Eq. (12) is used for all fits, the off-shell parameters are refitted for each different deuteron wave function model. The fitted off-shell functions δf^N are shown in Fig. 6 for the four wave function models considered. The off-shell corrections for the AV18, CD-Bonn and WJC-2 models have similar shapes: quite small at low x but becoming more positive at larger x. The function δf^N for these models has zero crossings at $x = x_1 \approx 0.05$ and $x = x_0 \approx 0.3$. For the WJC-1 model, on the other hand, the off-shell function is similar in magnitude, but has a shape that is somewhat orthogonal to the others. In this case it becomes more negative for $x \gtrsim 0.5$, with the parameter $x_1 \approx 0.15$, while the other zero crossing parameter is negative, $x_0 \approx -0.25$.

To test the sensitivity of the fit to the off-shell model, we also consider the more micro-

scopic OCS model for the off-shell function δf^N discussed in Sec. II D 2.

The rescaling parameter $\partial \log \Lambda^2 / \partial \log p^2$ evaluated at $p^2 = M^2$ is then included as a parameter in the fit, with errors propagated along with those of the other fit parameters in Tables II and III. ... (which involves one off-shell parameter instead of three for the parametrization in Eq. (12)

The results of the fit within the OCS model are displayed in Fig. 7 for various PDFs as ratios to the central CJ15 PDFs (computed using the off-shell parametrization (12) and the AV18 deuteron wave function). For the AV18, CD-Bonn and WJC-2 wave functions, the effects of the more restrictive OCS model and relatively small and generally within the $\Delta\chi^2 = 1$ bands. The overall χ^2/dof value is 0.982 for both the AV18 and CD-Bonn wave functions, and 0.984 for the WJC-2 wave function. This is marginally higher than the results of the fit with the phenomenological off-shell parametrization in Eq. (12), and comes mostly from a slightly higher χ^2 values for the SLAC F_2^d and DØ charged lepton asymmetry data. For the WJC-1 wave function, the results for the d-quark PDF show significantly greater deviation at large x, again suggesting that the hard tail of its momentum distribution is difficult to accommodate also within the OCS model, with a total χ^2/dof of 0.989. In addition, for the u-quark distribution the WJC-1 result lies slightly outside the uncertainty band at $x \sim 0.05$.

We should note, however, that the off-shell correction term δf^N, or even the off-shell PDF $\widetilde{q}^N$ in Eq. (8), alone is unphyiscal. Only the convolution of $\widetilde{q}^N$ with the smearing function $f_{N/d}$ in Eq. (7) corresponds to the physical deuteron parton distribution (or structure function), and the two corrections (deuteron wave function and nucleon off-shell) must always be considered together. Since the off-shell correction is fitted, changes in deuteron wave function can in practice be compensated by a corresponding change in the off-shell parameters, to the extent allowed by the specific choice of wave function and off-shell parametrization. This is clearly illustrated in Fig. 8, where the deuteron EMC ratio F_2^d/F_2^N is shown for the four different wave functions considered, and the 3-parameter off-shell parametrization in Eq. (12). Remarkably the structure function ratio is almost idential for the AV18, CD-Bonn and WJC-2 models, while the WJC-1 result differs slightly from these, reflecting the observations in Figs. 5–7 above.

In addition to the important role played by nuclear corrections in F_2^d at large values of x, the effects of finite-Q^2 corrections are also significant, especially at low Q^2. In an

earlier study [11], a nontrivial interplay was observed between the kinematical TMCs and the dynamical higher twist corrections parametrized in Eq. (5). The impact of the finite-Q^2 corrections on the F_2^d/F_2^N ratio is illustrated in Fig. 9 for the CJ15 fit, for Q^2 between 2 GeV^2 and 100 GeV^2. The rise in the ratio at large x is fastest at the highest Q^2 value, and becomes less steep with decreasing Q^2. The general shape remains independent of the scale for $Q^2 \gtrsim 5$ GeV^2, however, a dramatic change occurs at $Q^2 \sim 2$ GeV^2, where F_2^d/F_2^N rises slowly until $x \approx 0.75$ before abruptly turning down for larger x. This behavior arises from the interplay between the TMCs to the free and smeared nucleon structure functions, and the Q^2 dependent corrections to the smearing functions $f_{N/d}$ at finite values of x^2/Q^2.

For the standard TMC prescription adopted in this analysis, namely that based on the operator product expansion [52], the fitted higher twist coefficient function $C_{\rm HT}$ in Eq. (6) is plotted in Fig. 10, with the parameters given in Table III for the CJ15 fit. The coefficient displays the characteristic rise at large values of x observed in previous higher twist extractions, and is almost completely independent of the deuteron wave function model for the entire range of x considered.

C. d/u ratio

The nuclear and finite-Q^2 corrections that manifest themselves in the F_2^d/F_2^N ratio as observed in Figs. 8 and 9 directly translate into modifying the behavior of the d/u PDF ratio at large x. Our previous analyses [11, 14, 15] have made detailed studies of the relationship between the size of the nuclear corrections in the deuteron and the shape and $x \to 1$ limit of d/u. For the CJ12 PDFs [15], three sets of nuclear corrections were considered, corresponding to mild, medium and strong nuclear corrections, and referred to as "CJ12min", "CJ12mid" and "CJ12max", respectively. Each of these sets was consistent with the available data constraints, and provided a convenient way to explore the nuclear effects on various observables.

Since our last analysis, new data on charged lepton [32, 33] and W boson asymmetries [35] over a large range of rapidities have become available from the DØ collaboration, which place significant constraints on the d/u ratio at high x. The new DØ electron and muon asymmetry data, together with earlier data from CDF [31], are displayed in Fig. 11 as a function of the lepton pseudorapidity η_l and compared with the CJ15 fit. Compared with

the range of nuclear corrections in CJ12, the lepton asymmetry data, and especially the new results from DØ [32, 33], strongly favor a smaller nuclear correction at large x, closer to the CJ12min set.

The extracted W boson asymmetries, which are more directly related to the shape of the PDFs, are shown in Fig. 12 as a function of the W boson rapidity y_W. The statistical errors bars on the DØ e and μ data in particular are extremely small and place severe constraints on the fit. The χ^2/dof for the DØ lepton asymmetries are ≈ 2, although the overall fit the data in Fig. 11 is good. The earlier CDF electron data have larger errors and give a $\chi^2/\text{dof} \approx 1$. The fit to the extracted W asymmetries gives $\chi^2/\text{dof} \approx 1$ for both the CDF and DØ data.

The stronger constraints from the charge asymmetry data leads to a significant reduction in the uncertainties on the d/u ratio, particularly at large values of x. This is illustrated in Fig. 13, which demonstrates the shrinking of the d/u uncertainty bands (which are shown here with a tolerance of $T = 10$) with the successive addition of various data sets. Compared with the fit to DIS only data, in which the d/u ratio has very large uncertainties beyond $x \approx 0.4$, the addition of the lepton asymmetries leads to a reduction in d/u of more than a factor 2 at both small x and large x. (Addition of Z boson rapidity data [36, 37] has only modest impact on d/u.) Subsequent inclusion of the W asymmetries leads to a further halving of the uncertainty at $x \approx 0.6 - 0.8$, while having minimal effect on the errors at $x \lesssim 0.4$.

In fact, independent of the charge asymmetry data, a significant reduction in the d/u uncertainty at intermediate x values is already provided by the new Jefferson Lab data on the neutron to deuteron ratio F_2^n/F_2^d from the BONuS collaboration [89]. While the BONuS data have little or no effect at $x \lesssim 0.3$, the reduction in the d/u error at $x \sim 0.5 - 0.6$ is almost as large as that from the lepton asymmetries. Curiously, the BONuS data have a slight preference for stronger nuclear corrections, in contrast to the lepton asymmetry data, although the tension is not significant. Using all the available data from DIS and W boson production, the central value of the extrapolated d/u ratio at $x = 1$ is ≈ 0.1 at the input scale Q_0^2. The nuclear model dependence of the central values of the $x \to 1$ limit of d/u is relatively weak, ranging from 0.08 for the WJC-1 wave function to 0.12 for the CD-Bonn model.

While the new charge asymmetry and BONuS F_2^n/F_2^d data provide significant constraints

on the d/u ratio, the existing inclusive deuteron DIS data still play an important role in global analyses, as does the proper treatment of the nuclear corrections. If one were to fit F_2^d data without accounting for nuclear effects (assuming $F_2^d = F_2^p + F_2^n$), the resulting d/u ratio would be strongly overestimated beyond $x = 0.6$, where the nuclear EMC ratio begins to deviate significantly from unity (see Fig. 8). This is illustrated in Fig. 14, where the CJ15 d/u ratio is compared with the fit without nuclear corrections. This behavior can be understood from the shape of the F_2^d/F_2^N ratio Fig. 8 at large x, where the effect of the nuclear corrections is to increase the ratio above unity for $x \gtrsim 0.6$. Since F_2^d and F_2^p are fixed inputs, a larger F_2^d/F_2^N is generated by a smaller neutron F_2^n and hence a smaller d/u ratio. For example, the effect of the nuclear corrections is to shift the d/u ratio at $x = 0.8$ from the ($T = 10$) range $\approx 0.1 - 0.3$ to $\approx 0 - 0.2$ once the smearing and off-shell effects are included. Removing the deuterium data altogether increases the overall uncertainty band for $x \gtrsim 0.7$. Surprisingly, the deuteron data also reduce the d/u uncertainties slightly at smaller x, $0.05 \lesssim x \lesssim 0.15$.

Effects on large-x PDFs from nuclear corrections have also been investigated by several other groups in recent years [17, 19, 46, 47, 49, 82], and it is instructive to compare the CJ15 results on the d/u ratio with those analyses. The MMHT14 fit [17] uses a purely phenomenological nuclear correction for the combined effects of nuclear smearing and off-shell corrections, in contrast to our approach in which the (poorly understood) off-shell correction is fitted but the (better known) deuteron wave function correction is computed. Interestingly, the phenomenological MMHT14 nuclear correction has a qualitatively similar shape to that found in our more microscopic estimate. For $x \lesssim 0.7$ the MMHT14 d/u uncertainty is comparable to that in CJ15 with $T = 10$, although for $x \gtrsim 0.8$ the uncertainty diverges rapidly due to the different error evaluation methodologies used.

The JR14 analysis [49] uses similar smearing functions to those used in our fit, but does not include nucleon off-shell corrections. Furthermore, it uses the $\Delta\chi^2 = 1$ criterion for the 1-σ confidence level, based on statistical considerations alone, but introduces additional systematic uncertainties through the dependence of the fit on the input scale. The resulting uncertainty on d/u is larger than that in CJ15 in the intermediate-x region, which may reflect the absence of the recent W and lepton asymmetry data in the JR14 fit. The range of d/u values extrapolated to $x = 1$ is similar to the CJ15 band within errors (for $T = 10$), although the form of the JR14 parametrization forces $d/u \to 0$ at $x = 1$.

The CJ15 uncertainty band in Fig. 15 is also similar to that found in the CT14 global analysis [18], which does not apply any nuclear corrections to deuterium data, on the basis of the somewhat higher W^2 cuts utilized. The CT14 analysis uses a parametrization based on Bernstein polynomials multiplying a common factor $x^{a_1}(1-x)^{a_2}$, and fixes the exponents a_2 to the same for the u- and d-quark PDFs, thereby allowing finite values of the d/u ratio in the $x \to 1$ limit. The results of the two analyses largely overlap over much of the x range, with the CT14 distributions being slightly above the CJ15 error band at $x \gtrsim 0.6$. This is reminiscent of the higher d/u ratio observed in Fig. 14 when the nuclear corrections are switched off.

...[ANYTHING ELSE TO BE SAID ABOUT d/u COMPARISONS/ OTHER ANALYSES?]...

V. CONCLUSION

[XXX editing]

In this paper we have ...

Acknowledgments

We thank M. E. Christy, P. Monaghan, ... for for helpful discussions. This work was supported by the DOE contract No. DE-AC05-06OR23177, under which Jefferson Science Associates, LLC operates Jefferson Lab. The work of J.F.O. and A.A. was supported in part by DOE contracts No. DE-FG02-97ER41922 and No. DE-SC0008791, respectively.

---

[1] W. Melnitchouk and A. W. Thomas Phys. Rev. D **47**, 3783 (1993).

[2] B. Badelek and J. Kwiecinski, Nucl. Phys. **B370**, 278 (1992).

[3] L. P. Kaptari and A. Yu. Umnikov, Phys. Lett. B **272**, 359 (1991).

[4] R. P. Feynman, *Photon Hadron Interactions* (Benjamin, Reading, Massachusetts, 1972).

[5] F. E. Close, Phys. Lett. B **43**, 422 (1973).

[6] G. R. Farrar and D. R. Jackson, Phys. Rev. Lett. **35**, 1416 (1975).

[7] W. Melnitchouk and A. W. Thomas, Phys. Lett. B **377**, 11 (1996).

[8] R. J. Holt and C. D. Roberts, Rev. Mod. Phys. **82**, 2991 (2010).

[9] S. Kuhlmann *et al.*, Phys. Lett. B **476**, 291 (2000).

[10] L. T. Brady, A. Accardi, W. Melnitchouk and J. F. Owens, JHEP **1206**, 019 (2012).

[11] A. Accardi, M. E. Christy, C. E. Keppel, P. Monaghan, W. Melnitchouk, J. G. Morfin and J. F. Owens, Phys. Rev. D **81**, 034016 (2010).

[12] J. Arrington, F. Coester, R. J. Holt and T.-S. H. Lee, J. Phys. G **36**, 025005 (2009).

[13] J. Arrington, J. G. Rubin and W. Melnitchouk, Phys. Rev. Lett. **108**, 252001 (2012).

[14] A. Accardi, W. Melnitchouk, J. F. Owens, M. E. Christy, C. E. Keppel, L. Zhu and J. G. Morfin, Phys. Rev. D **84**, 014008 (2011).

[15] J. F. Owens, A. Accardi and W. Melnitchouk, Phys. Rev. D **87**, 094012 (2013).

[16] The CTEQ-Jefferson Lab (CJ) collaboration website, http://www.jlab.org/cj.

[17] L. A. Harland-Lang, A. D. Martin, P. Motylinski and R. S. Thorne, Eur. Phys. J. C **75**, 204 (2015).

[18] S. Dulat *et al.*, arXiv:1506.07443 [hep-ph].

[19] R. D. Ball *et al.*, Phys. Lett. B **723**, 330 (2013).

[20] R. D. Ball *et al.*, JHEP **1504**, 040 (2015).

[21] F. D. Aaron *et al.*, JHEP **1001**, 109 (2010).

[22] V. Radescu, arXiv:1308.0374.

[23] A. C. Benvenuti *et al.*, Phys. Lett. B **223**, 485 (1989); *ibid.* B **236**, 592 (1989).

[24] M. Arneodo *et al.*, Nucl. Phys. B **483**, 3 (1997).

[25] M. Arneodo *et al.*, Nucl. Phys. B **487**, 3 (1997).

[26] L. W. Whitlow *et al.*, Phys. Lett. B **282**, 475 (1992).

[27] S. P. Malace *et al.*, Phys. Rev. C **80**, 035207 (2009).

[28] F. D. Aaron *et al.*, JHEP **1001**, 109 (2010).

[29] E. A. Hawker *et al.*, Phys. Rev. Lett. **80**, 3715 (1998); J. Webb, Ph.D. Thesis, New Mexico State University (2002), arXiv:hep-ex/0301031; P. Reimer, private communication, `http://p25ext.lanl.gov/e866/papers/e866dyabs/E866_Drell-Yan_Cross_Sections/E866_Drell-Yar`

[30] R. S. Towell *et al.*, Phys. Rev. D **64**, 052002 (2001).

[31] D. Acosta *et al.*, Phys. Rev. D **71**, 051104(R) (2005).

[32] V. M. Abazov *et al.*, Phys. Rev. D **91**, 032007 (2015).

[33] V. M. Abazov *et al.*, Phys. Rev. D **88**, 091102 (2013).

[34] T. Aaltonen *et al.*, Phys. Rev. Lett. **102**, 181801 (2009).

[35] V. M. Abazov *et al.*, Phys. Rev. Lett. **112**, 151803 (2014) [Phys. Rev. Lett. **114**, 049901 (2015)].

[36] T. Aaltonen *et al.*, Phys. Lett. B **692**, 232 (2010).

[37] V. M. Abazov *et al.*, Phys. Rev. D **76**, 012003 (2007).

[38] T. Affolder *et al.*, Phys. Rev. D **64**, 032001 (2001).

[39] T. Aaltonen *et al.*, Phys. Rev. D **78**, 052006 (2008).

[40] B. Abbott *et al.*, Phys. Rev. Lett. **86**, 1707 (2001).

[41] V. M. Abazov *et al.*, Phys. Rev. Lett. **101**, 062001 (2008).
B. Abbott *et al.*, Phys. Rev. Lett. **86**, 1707 (2001).

[42] V. M. Abazov *et al.*, Phys. Lett. B **666**, 435 (2008).

[43] D. Mason *et al.*, Phys. Rev. Lett. **99**, 192001 (2007).

[44] G. Aad *et al.*, Phys. Rev. Lett. **109**, 012001 (2012).

[45] G. Moreno *et al.*, Phys. Rev. D **43**, 2815 (1991). ...[IS THIS CORRECT REFERENCE??]...

[46] S. Alekhin, J. Blümlein, S. Klein and S.-O. Moch, Phys. Rev. D **81**, 014032 (2010).

[47] S. Alekhin, J. Blümlein and S.-O. Moch, Phys. Rev. D **86**, 054009 (2012).

[48] A. D. Martin, W. J. Stirling, R. S. Thorne and G. Watt, Eur. Phys. J. C **63**, 189 (2009).

[49] P. Jimenez-Delgado and E. Reya, Phys. Rev. D **89**, 074049 (2014).

[50] P. Jimenez-Delgado, W. Melnitchouk and J. F. Owens, J. Phys. G: Nucl. Part. Phys. **40**, 093102 (2013).

[51] J. Beringer *et al.* [Particle Data Group Collaboration], Phys. Rev. D **86**, 010001 (2012), `http://pdg.lbl.gov`.

[52] H. Georgi and H. D. Politzer, Phys. Rev. D **14**, 1829 (1976).

[53] R. K. Ellis, R. Petronzio and G. Parisi, Phys. Lett. B **64**, 97 (1976).

[54] A. Accardi and J.-W. Qiu, JHEP **0807**, 090 (2008).

[55] A. Accardi, T. Hobbs and W. Melnitchouk, JHEP **0911**, 084 (2009).

[56] I. Schienbein *et al.*, J. Phys. G **35**, 053101 (2008).

[57] L. T. Brady, A. Accardi, T. J. Hobbs and W. Melnitchouk, Phys. Rev. D **84**, 074008 (2011) [Erratum-ibid. D **85**, 039902 (2012)].

[58] F. M. Steffens and W. Melnitchouk, Phys. Rev. C **73**, 055202 (2006).

[59] F. M. Steffens, M. D. Brown, W. Melnitchouk and S. Sanches, Phys. Rev. C **86**, 065208 (2012).

[60] A. De Rújula, H. Georgi and H. D. Politzer, Phys. Rev. D **15**, 2495 (1977).

[61] A. De Rújula, H. Georgi and H. D. Politzer, Ann. Phys. **103**, 315 (1977).

[62] M. Virchaux and A. Milsztajn, Phys. Lett. B **274**, 221 (1992).

[63] S. I. Alekhin, S. A. Kulagin and S. Liuti, Phys. Rev. D **69**, 114009 (2004).

[64] J. Blümlein and H. Böttcher, Phys. Lett. B **662**, 336 (2008).

[65] J. Blümlein, Prog. Part. Nucl. Phys. **69**, 28 (2013).

[66] W. Melnitchouk, A. W. Schreiber and A. W. Thomas, Phys. Rev. D **49**, 1183 (1994).

[67] S. A. Kulagin, G. Piller and W. Weise, Phys. Rev. C **50**, 1154 (1994).

[68] S. A. Kulagin, W. Melnitchouk, G. Piller and W. Weise, Phys. Rev. C **52**, 932 (1995).

[69] S. A. Kulagin and R. Petti, Nucl. Phys. A **765**, 126 (2006).

[70] Y. Kahn, W. Melnitchouk and S. A. Kulagin, Phys. Rev. C **79**, 035205 (2009).

[71] P. J. Ehlers, A. Accardi, L. T. Brady and W. Melnitchouk, Phys. Rev. D **90**, 014010 (2014).

[72] R. B. Wiringa, V. G. J. Stoks and R. Schiavilla, Phys. Rev. C **51**, 38 (1995).

[73] R. Machleidt, Phys. Rev. C **63**, 024001 (2001).

[74] F. Gross and A. Stadler, Phys. Rev. C **78**, 014005 (2008); *ibid.* C **82**, 034004 (2010).

[75] F. Gross and S. Liuti, Phys. Rev. C **45**, 1374 (1992).

[76] W. Melnitchouk, A. W. Schreiber and A. W. Thomas, Phys. Lett. B **335**, 11 (1994).

[77] H. Mineo, W. Bentz, N. Ishii, A. W. Thomas and K. Yazaki, Nucl. Phys. **A735**, 482 (2004).

[78] I. C. Cloet, W. Bentz and A. W. Thomas, Phys. Lett. B **642**, 210 (2006).

[79] W. Melnitchouk, M. Sargsian, and M. Strikman, Z. Phys. A **359**, 99 (1997).

[80] J. Pumplin *et al.*, JHEP **0207**, 012 (2003).

[81] The CTEQ collaboration website, http://www.cteq.org.

[82] A. D. Martin, A. J. Th. M. Mathijssen, W. J. Stirling, R. S. Thorne, B. J. A. Watt and G. Watt, Eur. Phys. J. C **73**, 2318 (2013).

[83] A. Accardi, AIP Conf. Proc. **1369**, 210 (2011).

[84] D. Stump *et al.*, JHEP **0310**, 046 (2003).

[85] J. Anderson [LHCb Collaboration], arXiv:1109.3371 [hep-ex].

[86] D. d'Enterria and J. Rojo, Nucl. Phys. **B860**, 311 (2012), arXiv:1202.1762[hep-ph].

[87] Y. Liang *et al.* [Jefferson Lab Hall C E94-110 Collaboration], arXiv:nucl-ex/0410027.

[88] P. Monaghan, A. Accardi, M. E. Christy, C. E. Keppel, W. Melnitchouk and L. Zhu, Phys. Rev. Lett. **110**, 152002 (2013).

[89] N. Baillie *et al.*, Phys. Rev. Lett. **108**, 142001 (2012); S. Tkachenko *et al.*, Phys. Rev. C **89**, 045206 (2014).

[90] Jefferson Lab Experiment C12-10-103 [MARATHON], G. G. Petratos, J. Gomez, R. J. Holt and R. D. Ransome, spokespersons.

[91] Jefferson Lab Experiment E12-10-102 [BONUS12], S. Bültmann, M. E. Christy, H. Fenker, K. Griffioen, C. E. Keppel, S. Kuhn and W. Melnitchouk, spokespersons.

[92] Jefferson Lab Experiment E12-10-007 [SoLID], P. Souder, spokesperson.

[93] P. Jimenez-Delgado, T. J. Hobbs, J. T. Londergan and W. Melnitchouk, Phys. Rev. Lett. **114**, 082002 (2015).

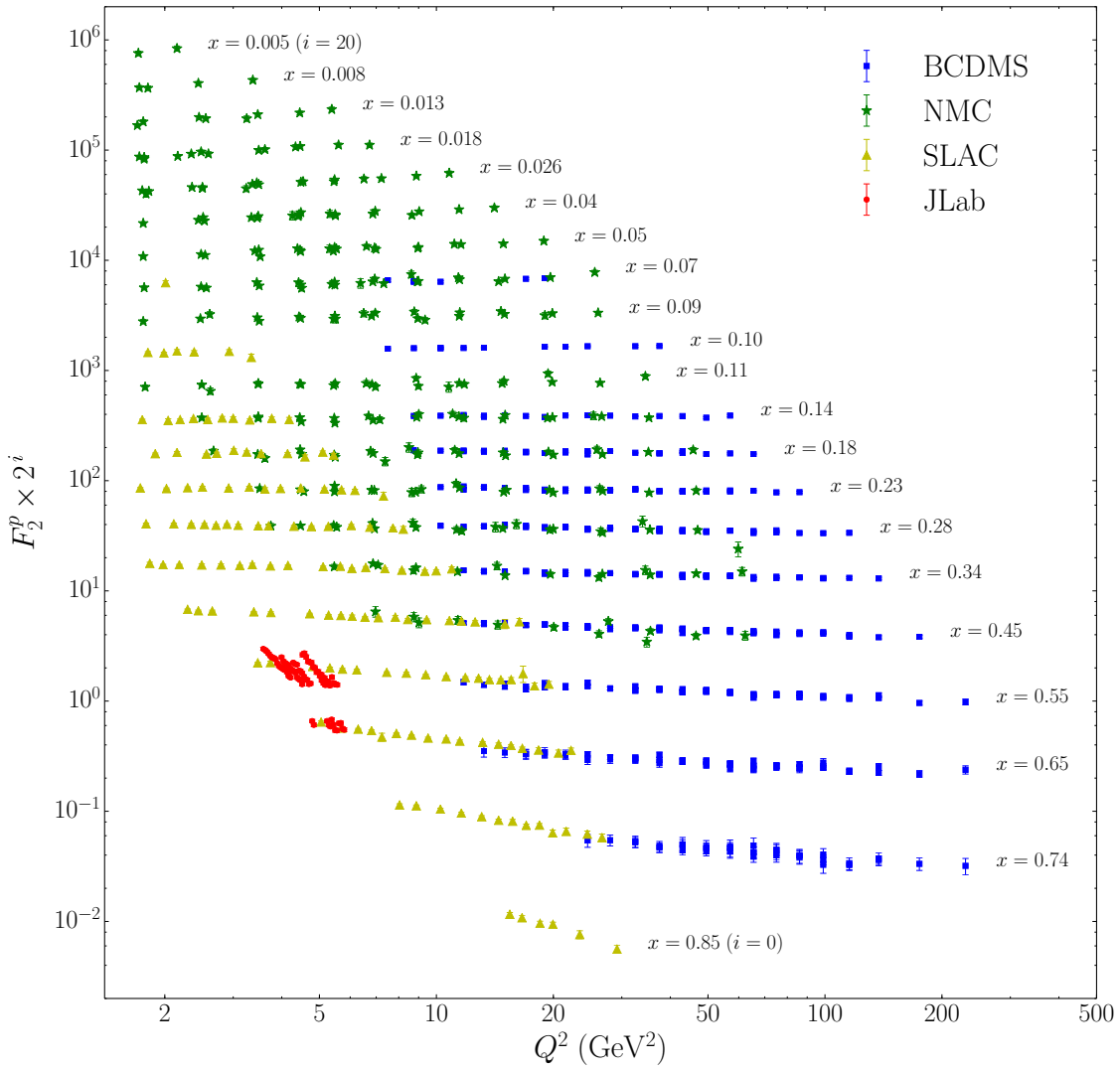

FIG. 1: Comparison of proton F_2^p structure function data from BCDMS [23], NMC [24], SLAC [26] and JLab [27] with the CJ15 NLO fit, for various Q^2 and x. The data at fixed x values have been scaled by a factor 2^i, from $i = 0$ for $x = 0.85$ to $i = 20$ for $x = 0.005$ in steps of $i = 1$.

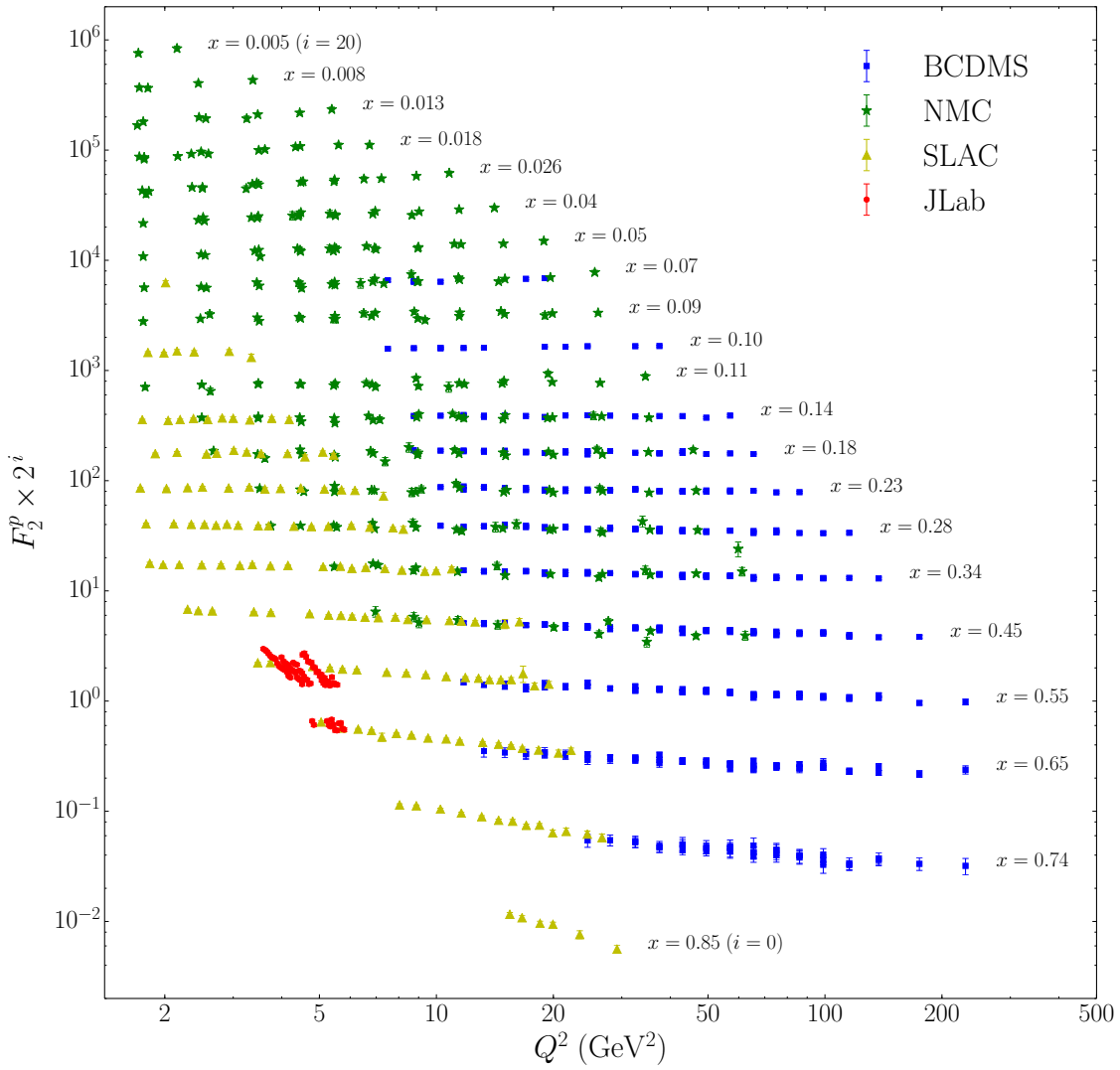

FIG. 2: [PLACEHOLDER FIGURE]... As for Fig. 1, but for the deuteron F_2^d structure function, illustrating data from BCDMS [23], SLAC [26] and JLab [27]. ...[WHAT TO DO WITH NMC F_2^d/F_2^p ?]...

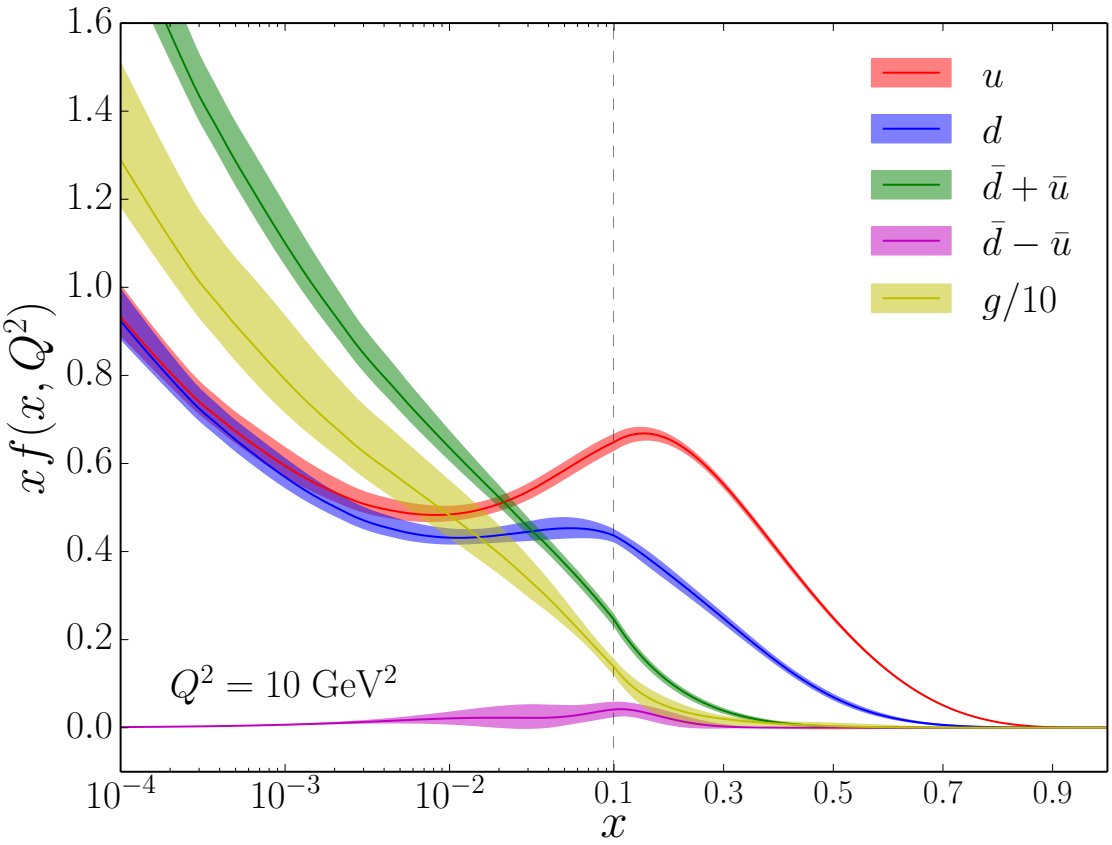

FIG. 3: Comparison of CJ15 PDFs for different flavors ($u, d, \bar{d}+\bar{u}, \bar{d}-\bar{u}$ and $g/10$) at a scale $Q^2 = 10$ GeV^2, for $T = 1$. Note the combined logarithimic/linear scale along the x-axis.

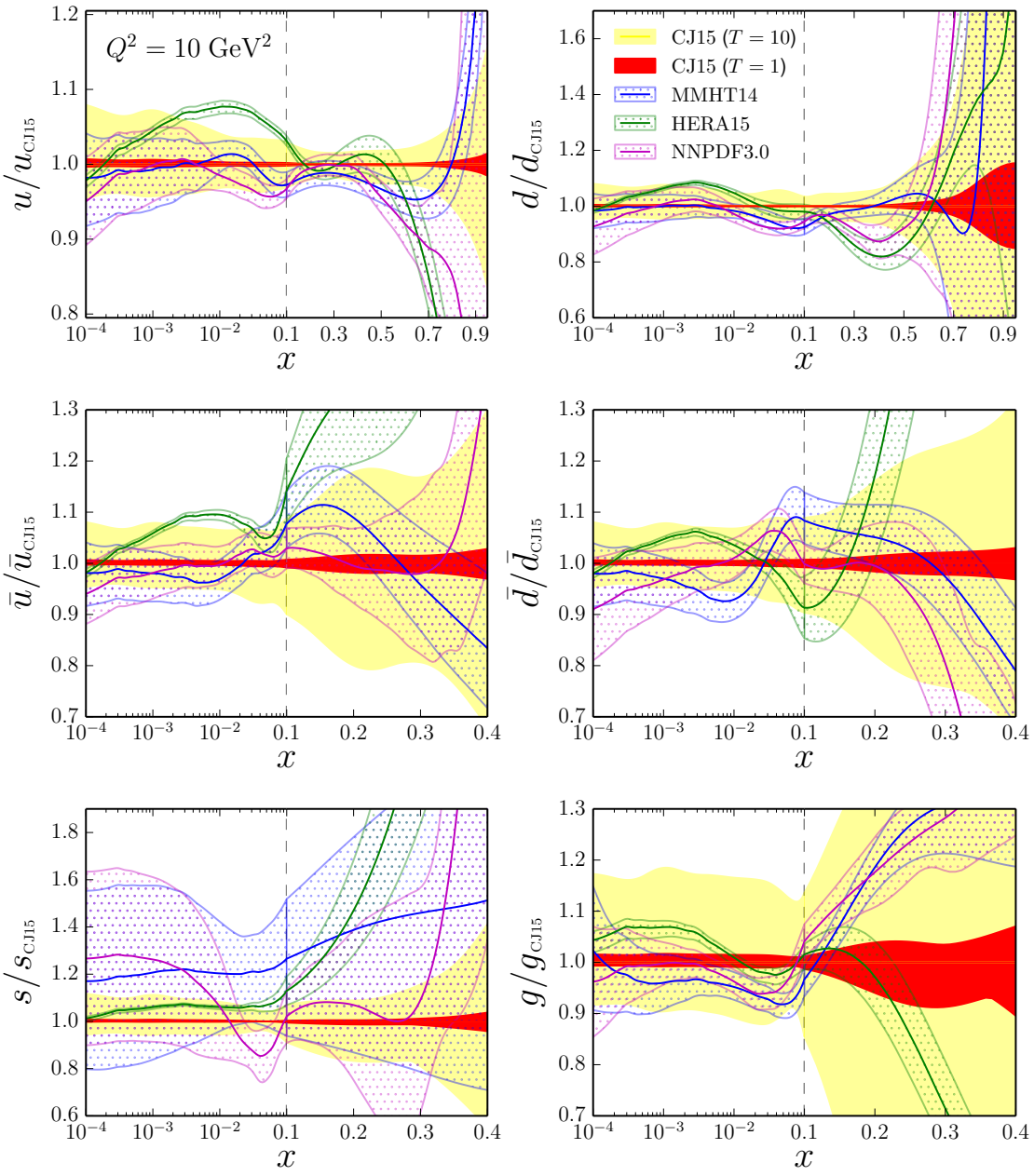

FIG. 4: Ratio of PDFs to the CJ15 central values for various PDF sets: CJ15 for tolerance $T = 1$ (red) and $T = 10$ (yellow), MMHT14 [17] (blue), HERAPDF15 [22] (green), and NNPDF3.0 [20] (magenta). Note the different scales on the vertical axes used for different flavors.

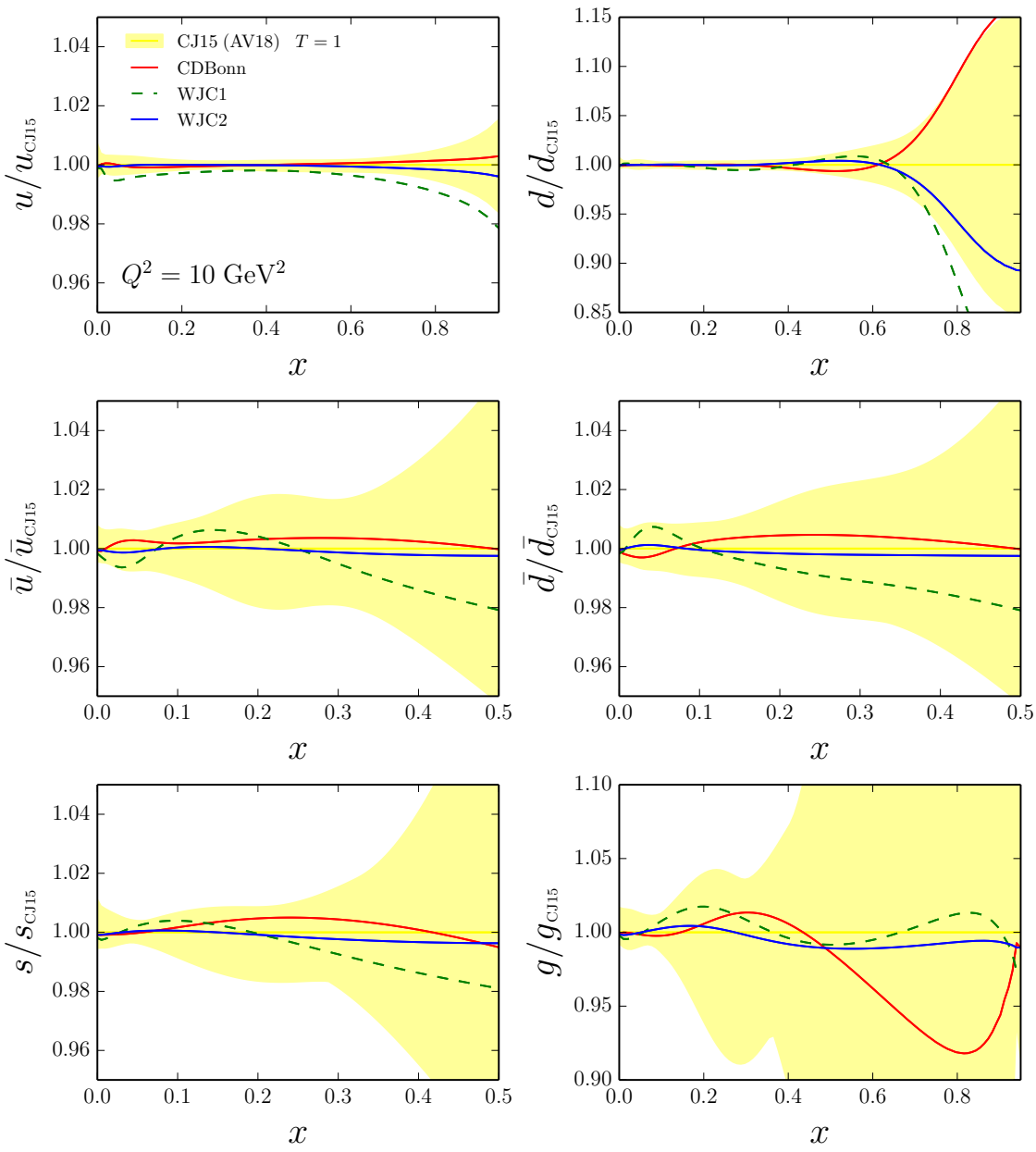

FIG. 5: Ratio of PDFs fitted using various deuteron wave function models to the CJ15 PDFs (which use the AV18 deuteron wave function): CD-Bonn (red solid lines), WJC-1 (green dashed lines), WJC-2 (blue solid lines). The CJ15 PDFs (yellow band) are shown for $T = 1$, and the off-shell parametrization (12) is used for all cases. Note the different scale on the vertical axes for the d-quark and gluon distributions.

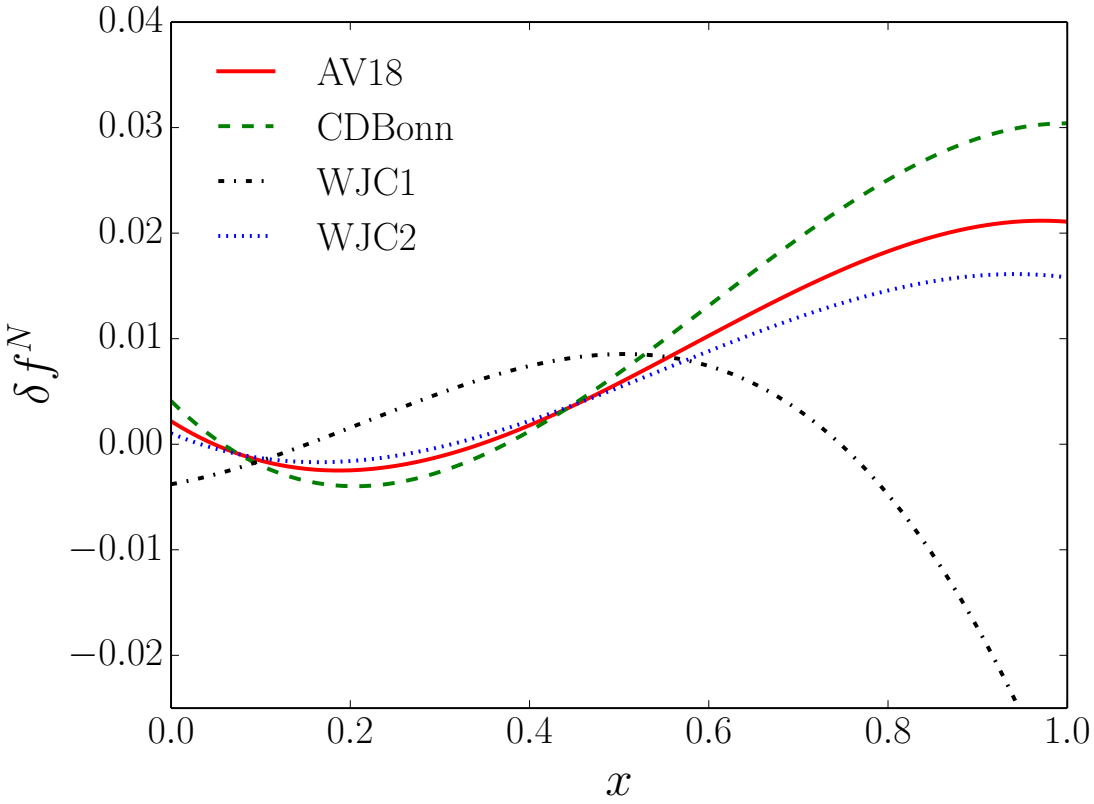

FIG. 6: Fitted nucleon off-shell correction δf^N for the parametrization in Eq. (12), using the AV18 (solid red line), CD-Bonn (dashed green line), WJC-1 (dot-dashed black line) and WJC-2 (dotted blue line) wave functions.

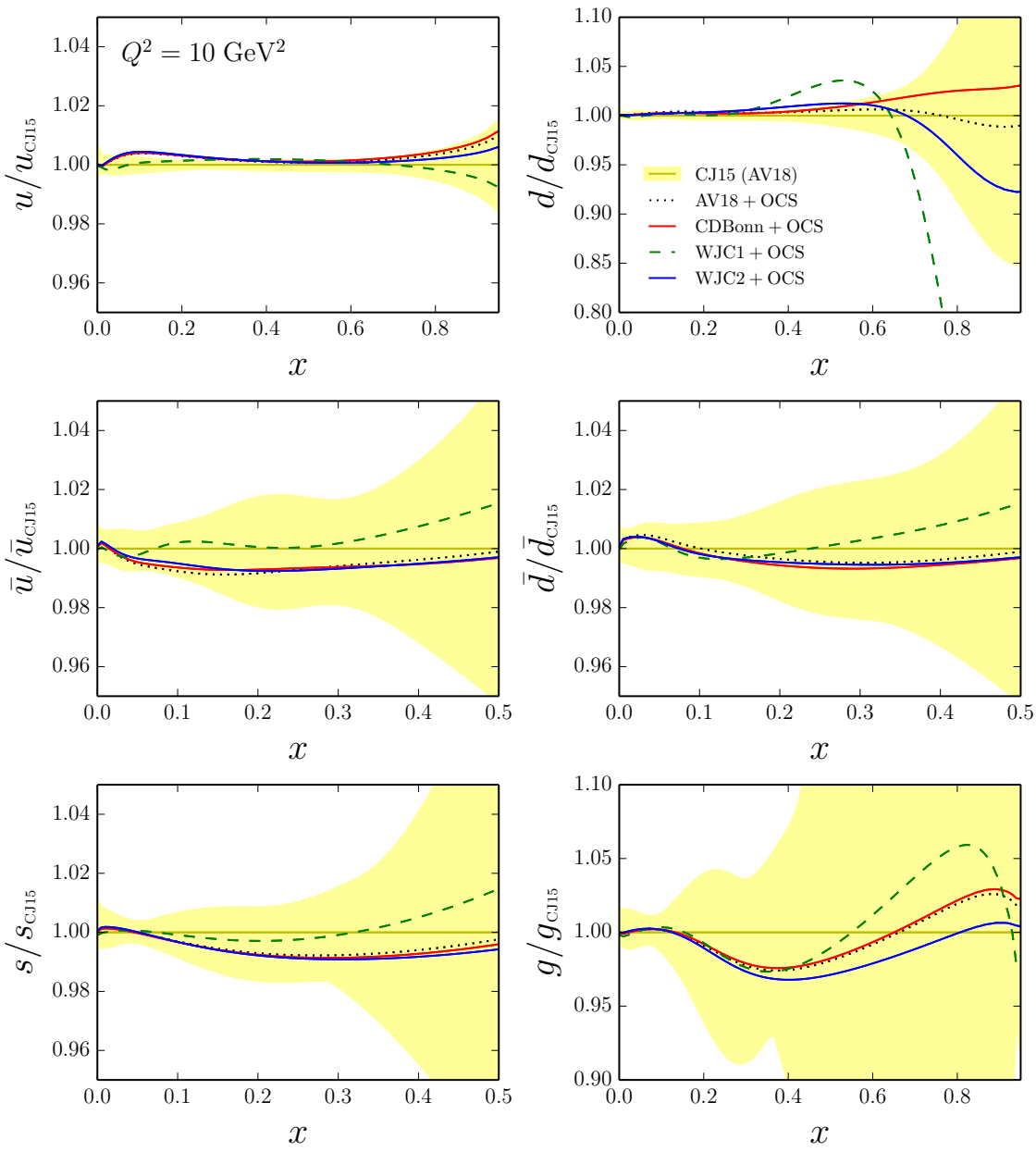

FIG. 7: Ratio of PDFs computed using the off-shell covariant spectator (OCS) model and different deuteron wave functions to the CJ15 PDFs (which use the off-shell parametrization (12) and the AV18 deuteron wave function): OCS model with the AV18 wave function (black dotted lines), CD-Bonn (red solid lines), WJC-1 (green dashed lines), and WJC-2 (blue solid lines). Note the different scale on the vertical axes for the d-quark and gluon distributions.

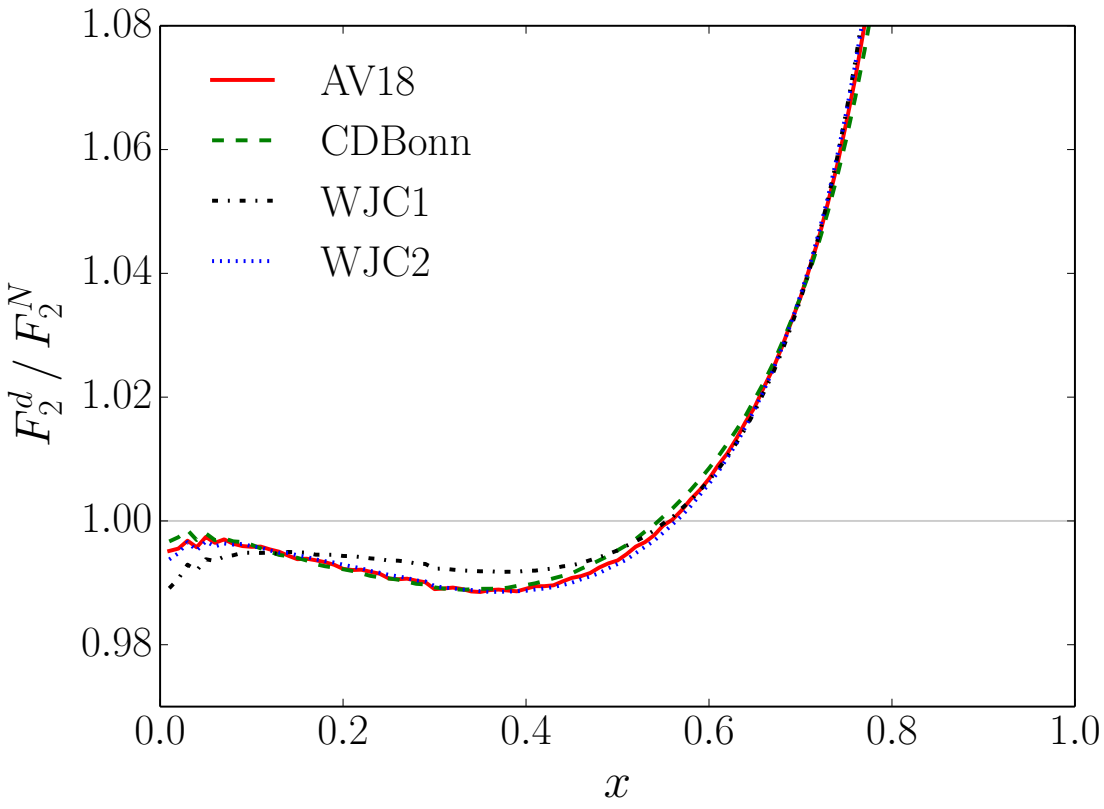

FIG. 8: Ratio of deuteron to isoscalar nucleon structure functions F_2^d/F_2^N for different deuteron wave function models at $Q^2 = 10$ GeV^2. ...[SMOOTH CURVES]...

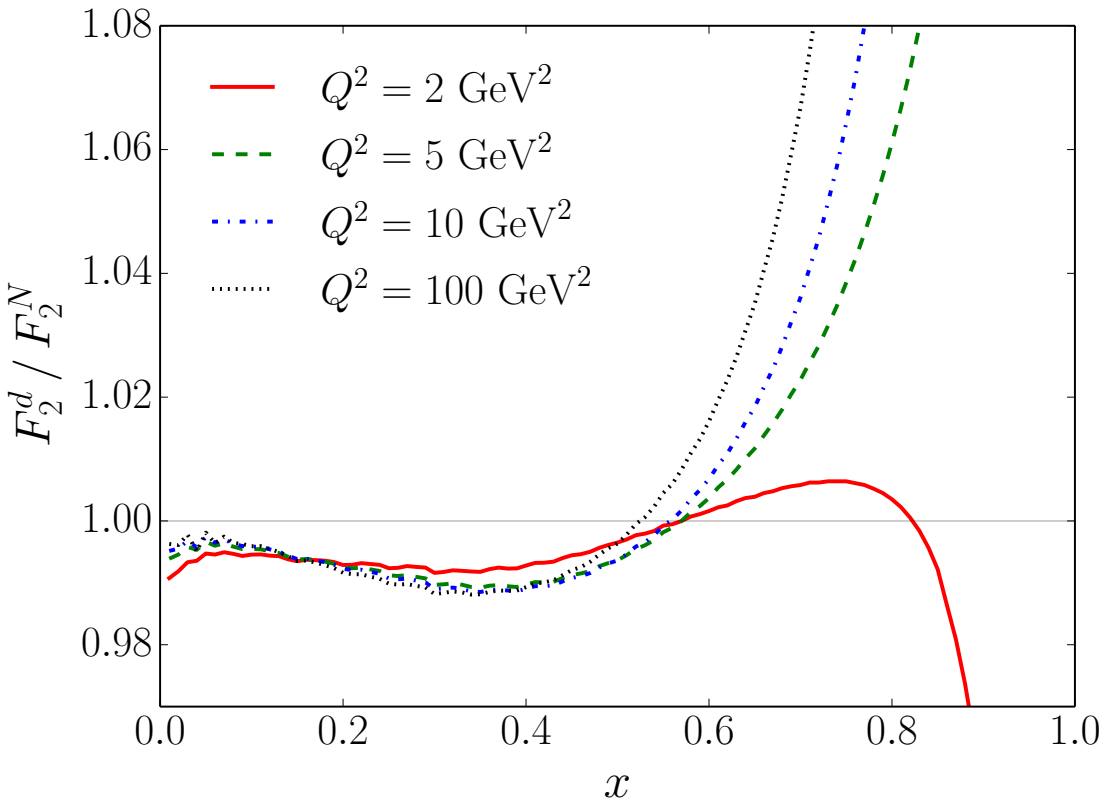

FIG. 9: Ratio of deuteron to isoscalar nucleon structure functions F_2^d/F_2^N computed from the CJ15 PDFs for different values of Q^2. ...[SMOOTH CURVES]...

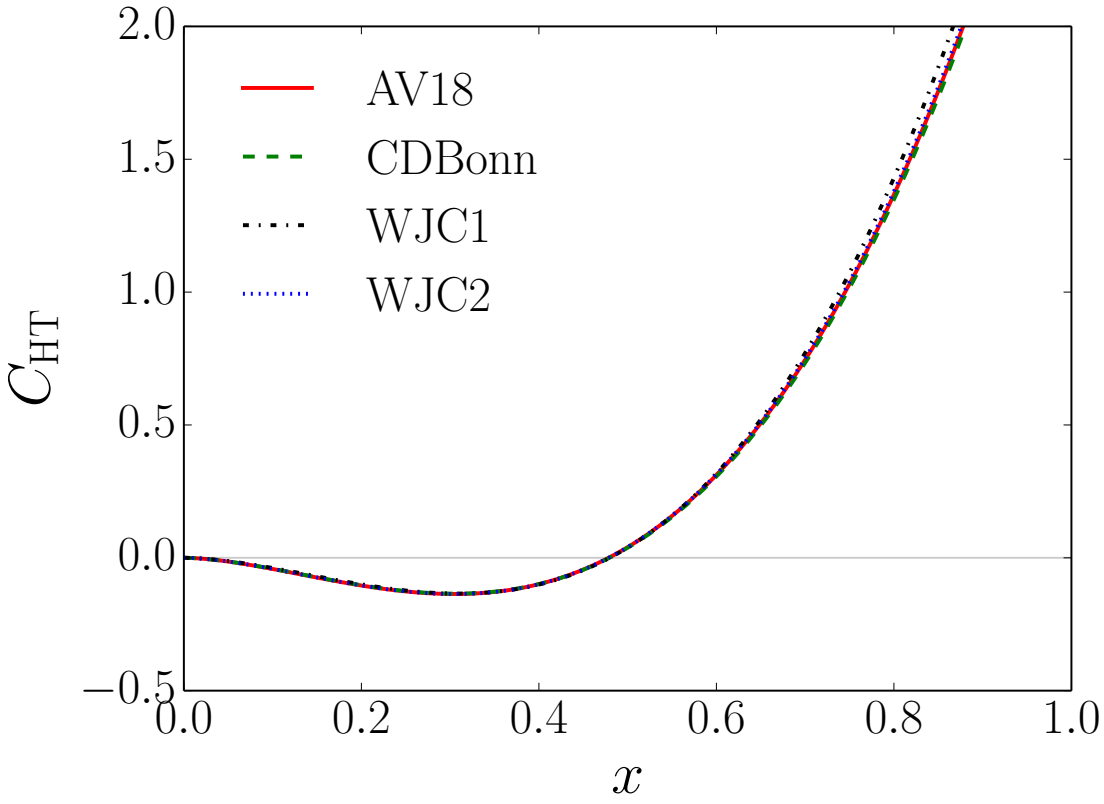

FIG. 10: Fitted higher twist function $C_{\rm HT}$ from Eq. (6), in units of GeV^2, for different deuteron wave function models.

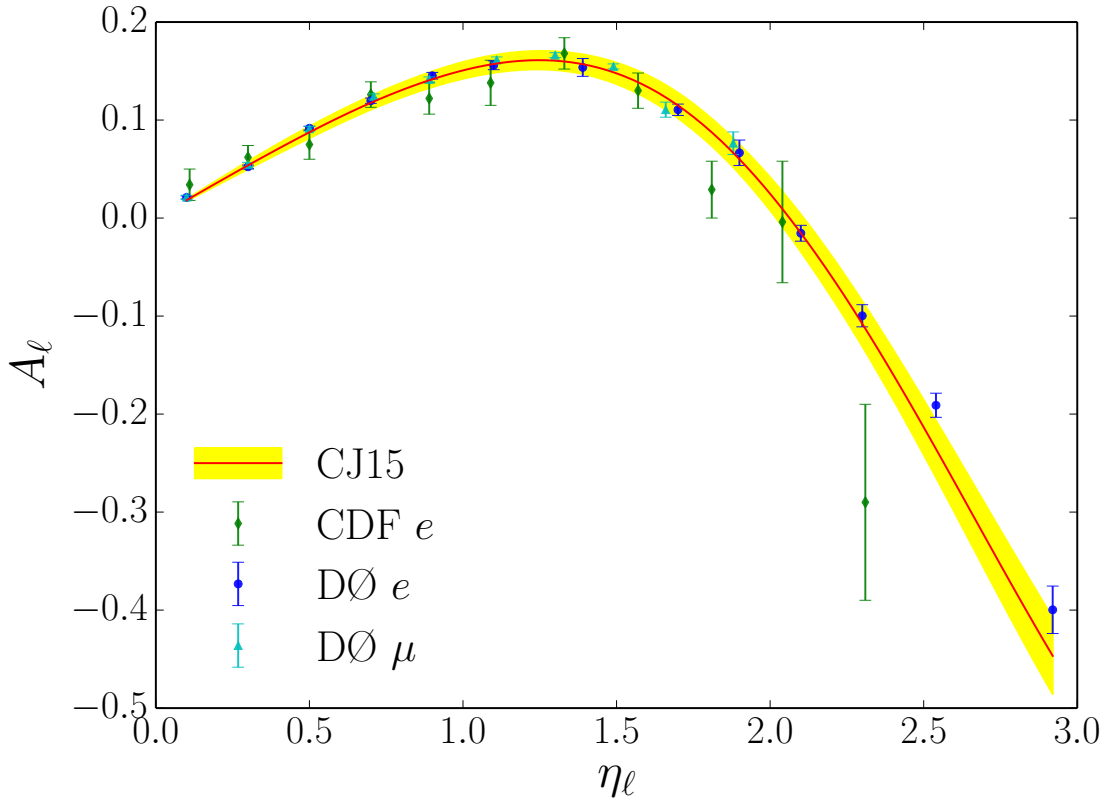

FIG. 11: Lepton charge asymmetry A_ℓ from $p\bar{p} \to WX \to \ell\nu X$ as a function of the lepton pseudorapidity η_ℓ from CDF electron (green diamonds) [31], and DØ electron (blue circles) [32] and muon (cyan triangles) [33] data compared with the CJ15 fit.

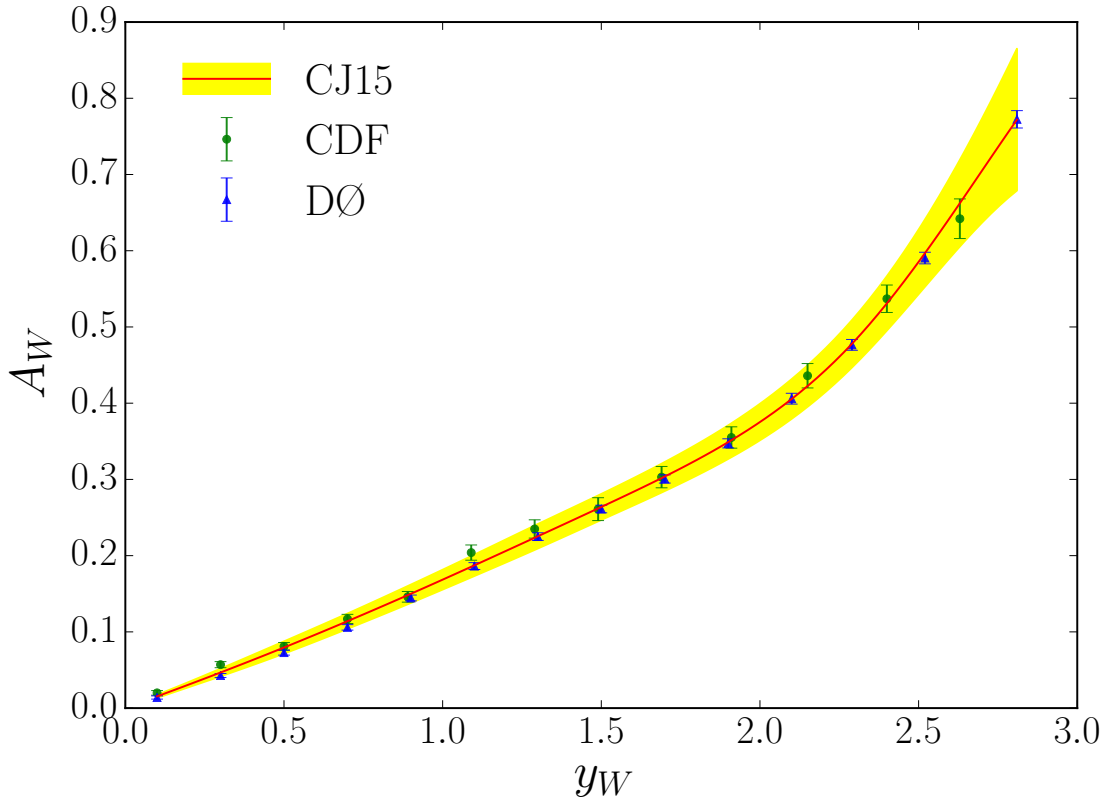

FIG. 12: W boson charge asymmetry A_W from $p\bar{p} \to WX$ as a function of the W boson rapidity y_W for CDF (green circles) [34] and DØ (blue triangles) [35] data compared with the CJ15 fit.

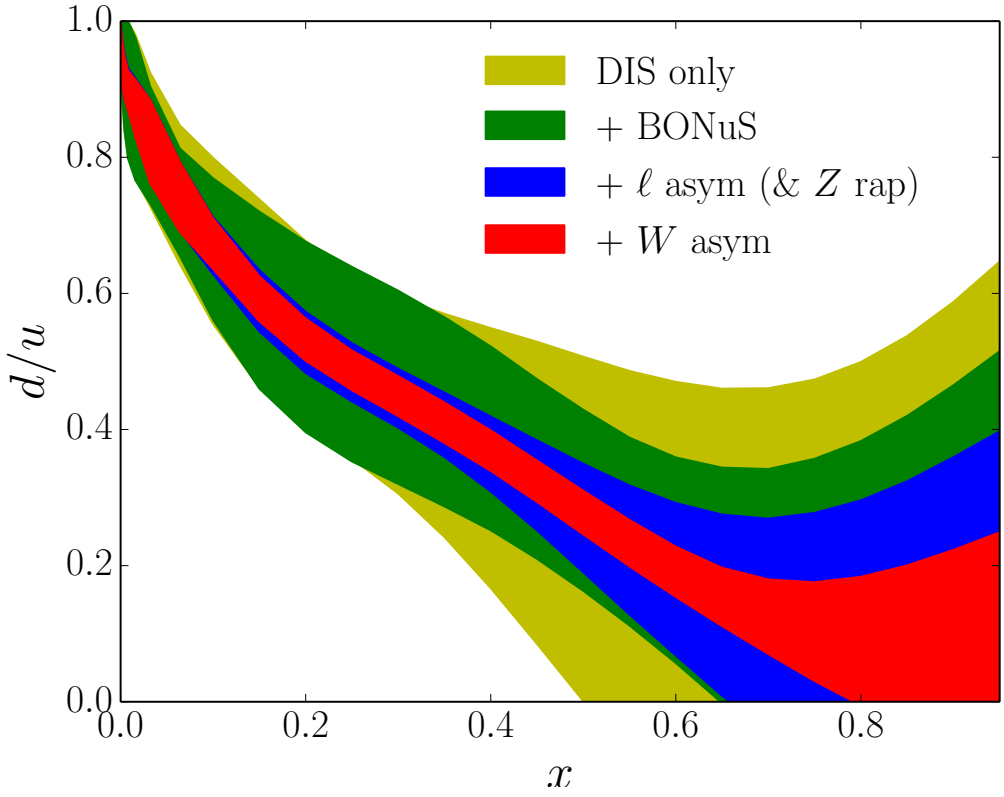

FIG. 13: Impact of various data sets on the d/u ratio at $Q^2 = 10$ GeV^2. The uncertainty band is largest for the DIS only data (yellow band), and decreases with the successive addition of JLab F_2^n/F_2^d [89] data (green band), lepton asymmetry [31–33] (and Z rapidity [36, 37]) data (blue band), and W boson asymmetry data [34, 35] (red band). ...[FIGURE NEEDS SMOOTHING]...

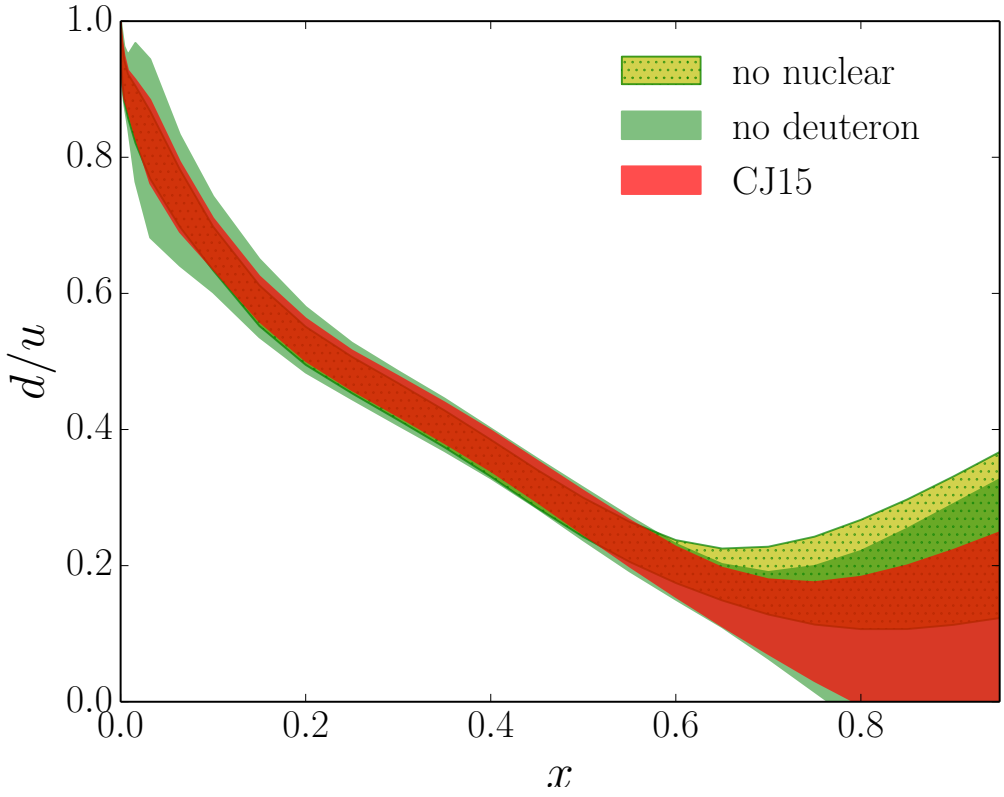

FIG. 14: Impact on the CJ15 d/u ratio (red band) of removing the deuterium nuclear corrections (yellow shaded band), and omitting the deuterium data (green band). ...[FIGURE NEEDS SMOOTHING]...

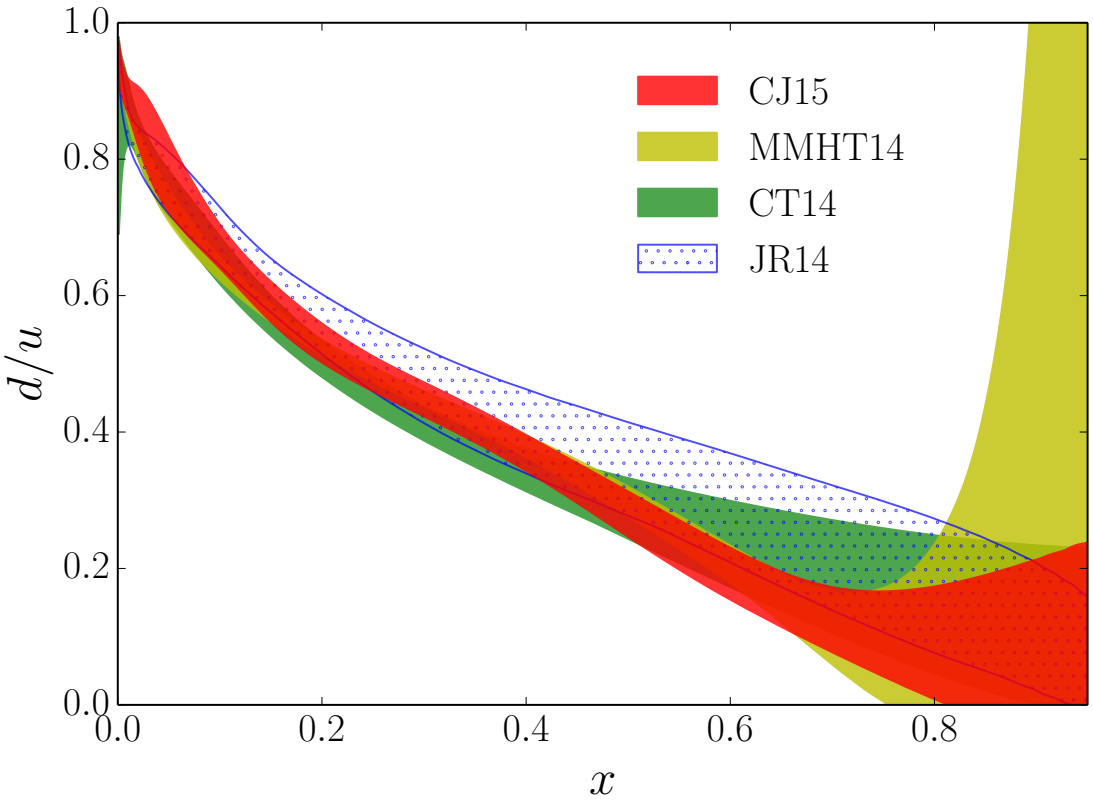

FIG. 15: Comparison of the d/u ratio at $Q^2 = 10$ GeV^2 for different PDF parametrizations: CJ15 (red band), MMHT14 [17] (yellow band), CT14 [18] (green band), and JR14 [49] (blue dotted band).

TABLE I: Data sets used in the CJ15 NLO global analysis (which uses the AV18 deuteron wave function and off-shell parametrization in Eq. (12), with the corresponding number of data points and the respective χ^2 values for each set. For comparison the χ^2 for the LO fit and for an NLO fit with the OCS off-shell model are also given. ...[remove LO & OCS entries?]...

	experiment	# points	χ^2		
			NLO	LO	NLO (OCS)
DIS F_2	BCDMS (p) [23]	351	437	432	435
	BCDMS (d) [23]	254	294	299	289
	NMC (p) [24]	275	407	414	406
	NMC (d/p) [25]	189	172	180	173
	SLAC (p) [26]	564	435	496	436
	SLAC (d) [26]	582	372	417	386
	JLab (p) [27]	136	166	164	166
	JLab (d) [27]	136	124	127	123
	JLab (n/d) [89]	191	217	224	215
DIS σ	HERA (NC e^-p) [28]	145	112	161	113
	HERA (NC e^+p) [28]	408	541	872	541
	HERA (CC e^-p) [28]	34	19	19	19
	HERA (CC e^+p) [28]	34	31	33	32
Drell-Yan	E605 (pCu) [45]	119	93	104	93
	E866 (pp) [29]	121	139	155	139
	E866 (pd) [29]	129	144	191	144
	E866 (pd/pp) [30]	12	9	9	8
W/charge asymmetry	CDF (e) [31]	11	12	11	12
	DØ (μ) [33]	10	20	21	29
	DØ (e) [32]	13	27	56	22
	CDF (W) [34]	13	15	12	15
	DØ (W) [35]	14	16	47	16
Z rapidity	CDF (Z) [36]	28	27	79	28
	DØ (Z) [37]	28	16	23	16
jet	CDF (run 2) [39]	72	15	22	15
	DØ (run 2) [41]	110	21	46	22
γ+jet	DØ 1 [42]	16	6	20	6
	DØ 2 [42]	16	15	40	15
	DØ 3 [42]	12	25	35	25
	DØ 4 [42]	12	13	77	13
total		4035	**3941**	4786	3952
total + norm			**3950**	4918	3961
χ^2/dof			**0.979**	1.219	0.982

TABLE II: Leading twist parameter values for the u_v, d_v, $\bar{d}+\bar{u}$, $\bar{d}-\bar{u}$ and g PDFs [Eq. (1)] from the CJ15 NLO analysis at the initial scale Q_0 GeV. Parameters without errors have been fixed. For the strange to non-strange sea quark PDF ratio [Eq. (4)], we take $\kappa = 0.4$. (The parameter values are given to 5 significant figures to avoid rounding errors.) ...[make neater/reduce sig. figs?]...

parameter	u_v	d_v	$\bar{d}+\bar{u}$	$\bar{d}-\bar{u}$	g
a_0	2.3585	23.233	0.14121 ± 0.0050459	35712	46.706
a_1	0.60985 ± 0.020299	1.1387 ± 0.034586	−0.21785 ± 0.0039454	3.9867 ± 0.049301	0.61586 ± 0.038277
a_2	3.5377 ± 0.011405	6.6180 ± 0.15977	8.4003 ± 0.14833	20.289 ± 0.66322	6.2335 ± 1.1222
a_3	0	−3.5743 ± 0.090782	0	17	−3.2703 ± 0.16746
a_4	3.5169 ± 0.42791	4.9133 ± 0.14586	16.055 ± 1.1403	49.881 ± 7.1398	3.0338 ± 0.31300
b	—	0.0042424 ± 0.00070691	—	—	—
c	—	2	—	—	—

TABLE III: Parameter values for the nucleon off-shell [Eq. (12)] and higher twist [Eq. (6)] corrections to F_2 from the CJ15 NLO analysis at the input scale Q_0^2. The off-shell parameters are fitted using the AV18 deuteron wave function. Parameters without errors have been fixed. (The parameter values are given to 5 significant figures to avoid rounding errors.)

parameter	value
C	0.098222 ± 0.028518
x_0	0.34487 ± 0.91982
x_1	0.048
h_0	−3.0094 ± 0.24080
h_1	1.7526 ± 0.10135
h_2	−2.0895 ± 0.026853